Exp Brain Res (2001) 136:60–72
DOI 10.1007/s002210000505

RESEARCH ARTICLE

Stefan Schaal · Dagmar Sternad

Origins and violations of the 2/3 power law in rhythmic three-dimensional arm movements

Received: 16 December 1999 / Accepted: 1 June 2000 / Published online: 15 November 2000

Abstract The 2/3 power law, the nonlinear relationship between tangential velocity and radius of curvature of the end-effector trajectory, is thought to be a fundamental constraint of the central nervous system in the formation of rhythmic endpoint trajectories. However, studies on the 2/3 power law have been confined largely to planar drawing patterns of relatively small size. With the hypothesis that this strategy overlooks nonlinear effects that are constitutive in movement generation, the present experiments tested the validity of the power law in elliptical patterns that were not confined to a planar surface and which were performed by the unconstrained 7-degrees of freedom (DOF) arm, with significant variations in pattern size and workspace orientation. Data were recorded from five human subjects where the seven joint angles and the endpoint trajectories were analyzed. Additionally, an anthropomorphic 7-DOF robot arm served as a "control subject" whose endpoint trajectories were generated on the basis of the human joint angle data, modeled as simple harmonic oscillations. Analyses of the endpoint trajectories demonstrate that the power law is systematically violated with increasing pattern size, in both exponent and the goodness of fit. The origins of these violations can be explained analytically based on smooth, rhythmic trajectory formation and the kinematic structure of the human arm. We conclude that, in unconstrained rhythmic movements, the power law seems to be a by-product of a movement system that favors smooth trajectories, and that it is unlikely to serve as a primary movement-generating principle. Our data rather suggest that subjects employed smooth oscillatory pattern generators in joint space to realize the required movement patterns.

S. Schaal (✉)
Computer Science and Neuroscience, HNB-103,
University of Southern California, Los Angeles, CA 90089-2520, USA
e-mail: sschaal@usc.edu
URL: http://www-slab.usc.edu/sschaal

D. Sternad
Department of Kinesiology, Pennsylvania State University,
266 Recreation Building, University Park, PA 16802, USA

S. Schaal · D. Sternad
Kawato Dynamic Brain Project (ERATO/JST), 2-2 Hikaridai,
Seika-cho, Soraku-gun, 619-02 Kyoto, Japan

Keywords Human arm movements · Rhythmic coordination · Trajectory formation · Power law · Smoothness · Human

Introduction

Invariant features of movement trajectories constitute an important window into understanding the fundamental organizing principles of biological motor control and the physiology of nervous systems. In the present work, we will examine one of these features, the 2/3 power law, with the goal of studying the mechanisms of rhythmic movement generation. Early studies by Viviani and Terzuolo (1980, 1982) on handwriting and drawing movements observed that there is a systematic relationship between the velocity of the end-effector trajectory and the geometric path[1] that it describes. This observation was quantified by Lacquaniti et al. (1983) as the "2/3 power law": the angular velocity $a(t)$ of the endpoint is proportional to the curvature $c(t)$ of the end-effector path by satisfying the power relation:

$$a(t)=kc(t)^{2/3}$$

Or equivalently:

$$\begin{aligned} v(t) &= kr(t)^{\beta} \text{ where } \beta = \frac{1}{3} \\ v(t) &= \|\dot{\mathbf{x}}(\mathbf{t})\| \text{ (tangential velocity)} \\ r(t) &= \frac{1}{c(t)} \text{ (radius of curvature)} \\ c(t) &= \sqrt{\frac{\|\dot{\mathbf{x}}(\mathbf{t})\|^2 \, \|\ddot{\mathbf{x}}(t)\|^2 - (\dot{\mathbf{x}}(\mathbf{t})^{\mathbf{T}}\ddot{\mathbf{x}}(t))^2}{\|\dot{\mathbf{x}}(t)\|^6}} \text{ (curvature)} \\ \mathbf{x}(t) &= [x(t), y(t), z(t)]^T \text{ (3D movement trajectory)} \end{aligned} \quad (1)$$

[1] It is important to keep in mind that a movement *path* denotes the spatial realization of a movement, irrespective of its timing, whereas a movement *trajectory* includes timing information. The quantitative description of movement paths is the topic of differential geometry (Morasso 1983); the radius of curvature is one such quantity.

The name "2/3 power law" originates from the formulation written in terms of angular velocity $a(t)$ and curvature $c(t)$ with the exponent 2/3. With a view to the data analysis, however, it is more convenient to use Eq. 1 for the tangential velocity $v(t)$ and radius of curvature $r(t)$ with power law exponent $\beta=1/3$. Hence, to avoid confusion, we will refer to the 2/3 power law simply as the power law. The factor k in Eq. 1 is a proportionality constant, also termed the "velocity gain factor" (Viviani and Cenzato 1985). To appreciate the appeal of the power law, one needs to emphasize that no physical reason exists why movement path and tangential velocity should be related.

Supporting evidence for the power law comes from numerous studies, ranging from experiments on skill development (Viviani and Schneider 1991), isometric force trajectories (Massey et al. 1992), and perceptuomotor tasks (Viviani and Mounoud 1990; Viviani and Stucchi 1989, 1992; Viviani et al. 1987) to results from population code activity in the cortex (Schwartz 1994). Given this converging support, the power law has become widely accepted as an important invariant in biological movement trajectories and even an evaluation criterion for the "goodness" of models (Harris and Wolpert 1998).

Yet, several studies have shown that the power law is not always accurate. For instance, in more complex (nonelliptical) movement patterns, movement segmentation needs to be assumed to retain its validity (Viviani and Cenzato 1985), and even in elliptical patterns systematic deviations can be observed (Osu 1993; Wann et al. 1988;). An alternative perspective was taken by Gribble and Ostry (1996), who demonstrated the validity of the power law but argued that it is primarily caused by neurophysiological and biomechanic properties and not the control mechanisms of the CNS.

The present study aims to find an explanation for the empirical phenomenon of the power law. Two hypotheses are examined: (1) The power law is an organizational principle for movement generation, implemented directly by the central nervous system; and (2) The power law is a by-product of other mechanisms of trajectory formation. For this purpose, we examined rhythmic, elliptical movements performed by the whole arm in three dimensions. Ellipses have always been patterns that reliably satisfied the power law, or at least in good approximation. In contrast to previous studies, however, we introduced significant size and workspace variations in our experiments. These conditions revealed strong violations of the power law in large patterns. Kinematic analyses of the human arm and smoothness arguments will allow us to reconcile our results with previous research, rendering the power law in rhythmic movement a by-product of smooth, oscillatory trajectory formation in joint space.

Materials and methods

The following experimental setup is largely the same as previously detailed by Sternad and Schaal (1999). We will thus describe only novel issues in this section and otherwise refer to our previous work.

Experimental strategy

To present our arguments, this study adopted the following strategy. First, human subjects performed cyclic drawing movements in three dimensions, i.e., without being constrained by a surface. Importantly, subjects used their whole arm and the patterns were scaled in size, shape, and orientation to examine the influence of the kinematics of the arm on the endpoint trajectory. Data were recorded from the endpoint and seven joint angles. Second, the joint angular trajectories were approximated by continuous sine waves, in agreement with the previous findings of Soechting et al. (1986) and Soechting and Terzuolo (1986). Third, based on these sinusoidal fits, the human joint movements were implemented and executed on a 7-degrees of freedom (DOF) anthropomorphic robot arm. Fourth, the hand paths of the robot produced by this control strategy were recorded in the same way as in the human experiments and were compared with those of the subjects. This methodology allowed the direct comparison of data from human subjects with data from an artificial system whose control strategy is known. Using a robot instead of a simulation enabled us to measure the artificial data with exactly the same devices as the human data, such that both data sets underwent the same distortions from data recording and data processing. In addition, the stringent constraints of an implementation on an actual robot helped assure the correctness of our statements and their applicability to a real anthropomorphic movement system.

Participants

Five volunteers from our laboratory (two women, three men) participated in the experiment. Their ages ranged between 24 and 38 years. All of them were right-handed and none reported any previous arm injuries. The experiments had been approved by the ethics committee, and subjects gave their informed consent prior to their inclusion in the study.

Data recording

Data recording was identical to our previous study (Sternad and Schaal 1999). In brief, six color markers attached to the subjects' arms were recorded at 60 Hz with a color vision-based motion-analysis system (Quickmag, Japan). The arrangement of the markers was such that joint angular data could be reconstructed robustly and that three-dimensional (3D) end-effector data were directly available, too.

Robot

As described by Sternad and Schaal (1999), we employed an anthropomorphic robot arm as a control subject. The arm had 7 DOF in a configuration that mimicked a human arm with a 3-DOF shoulder joint, a 1-DOF elbow, and a 3-DOF wrist joint. For control, the robot employed kinematic trajectory plans (joint position, velocity, and acceleration), converted those to joint torques by an inverse dynamics model based on estimated parameters (An et al. 1988), and executed the torque commands in conjunction with a low-gain PD controller. The lengths of the arm segments corresponded to those of a tall human being, with a total arm length of 0.94 m (shoulder to fingertip).

Procedure for the human experiments

After the subject were seated, they were instructed to draw a series of ellipses with their dominant arm in the transversal and frontal

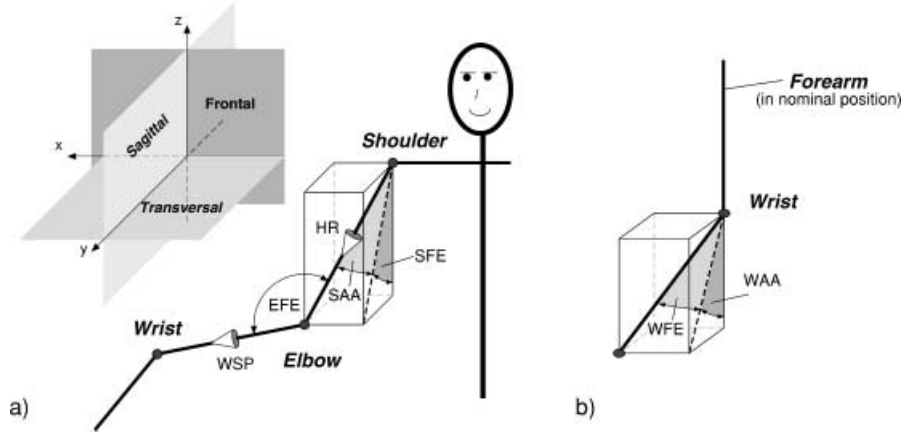

Fig. 1 **a** The coordinate system used for joint angles: shoulder flexion-extension (*SFE*) is the angle between the *z*-axis and the projection of the upper arm onto the sagittal plane; shoulder adduction-abduction (*SAA*) is the angle between the upper arm and the projection of the upper arm onto the sagittal plane; humeral rotation (*HR*) is the torsion angle about the upper arm; elbow flexion-extension (*EFE*) is the angle between upper and forearm in the plane spanned by the two limb segments; wrist supination-pronation (*WSP*) is the torsion angle about the forearm. **b** The wrist angles are defined relative to a nominal posture of the forearm and hand: the nominal posture is the forearm hanging straight down, while the palm is parallel to the sagittal plane and facing toward the body. Wrist flexion-extension (*WFE*) is the angle enclosed between the hand and the projection of the hand onto the sagittal plane; wrist adduction-abduction (*WAA*) is the angle between the *z*-axis and the projection of the hand onto the sagittal plane

plane. The experimenter demonstrated the elliptical patterns in their orientation with respect to the body and their approximate size. No extrinsic constraints were given that would confine the ellipse to a plane. A first set of transversal ellipses was drawn so that the long axis of the ellipse was approximately parallel to the *x*-axis (Fig. 1). A second set of transversal ellipses was drawn in a diagonal orientation, with the long axis pointing approximately from the center of the chest 45° to the right in the *x*-*y* plane. This diagonal orientation was chosen because joint limits are not so easily encountered as in other orientations (Viviani and Schneider 1991). Frontal ellipses were drawn in vertical and horizontal orientations, i.e., as a "standing" or a "lying" ellipse. The experimental trials were performed in four blocks, each consisting of ten trials, which were counterbalanced across participants. In one block, all elliptical patterns were performed in the same orientation and with approximately the same eccentricity, but at approximately five different sizes. Prior to the actual data collection, participants were asked to explore their workspace and practice different sizes of ellipses with the only constraint that for the largest patterns they should avoid extreme ranges of motion. The first trial of each block started with an intermediate-sized ellipse followed by ellipses in the following sequence of sizes (1 denotes the smallest and 5 denotes the largest ellipse, 3 is the intermediate size): 3, 4, 5, 3, 2, 1, 5, 4, 1, 2. This staggered order was chosen because participants could not remember the absolute sizes of the ellipses, and they also did not need to. By going through different sizes in this step-like fashion, all subjects could produce a roughly uniform distribution of different ellipses between a maximal and minimal size. Emphasis was placed on consistency in size and frequency of the patterns throughout the duration of one trial. For the actual data collection, subjects started the pattern, then they closed their eyes[2] to avoid visual orientation in Cartesian coordinates and, while continuing the pattern, they verbally signaled to the experimenter when they were ready for data recording. Data collection for one trial lasted for 15 s. Participants could rest their arms between trials whenever they needed to. The total experiment lasted approximately 30 min.

Data analysis

Data filtering

The three-dimensional trajectories of each marker were low-pass filtered using a zero-lag, second-order Butterworth filter with a 4.5-Hz cutoff frequency. For the analysis of the endpoint trajectory, the corresponding endpoint marker was additionally high-pass filtered with a second-order, zero-lag Butterworth filter (cutoff frequency 0.3 Hz). This filter eliminated slow drifts of the drawing pattern owing to the blindfolded pattern execution. After filtering, the first and last 60 data points of each trial were discarded to eliminate distortions from digital filter onsets. Smooth differential trajectories of each marker were obtained by a minimum jerk spline approximation, adapted from Wada and Kawato (1994). The reconstructed trajectories were guaranteed to lie within 0.01 m Euclidean distance from the measured trajectory; on average, they were within 0.001–0.002 m distance. The choice of all filter cutoff frequencies was the result of a pilot experiment using the robot arm. As the robot generated elliptical patterns, its fingertip data were recorded with the Quickmag system, a procedure that is obviously contaminated with some measurement noise. In addition, the joint angle data of the robot were recorded with high-resolution optical encoders, i.e., with very little measurement noise, such that the "true" fingertip position could be calculated from the known forward-kinematics model of the robot. By comparing the results of the power law analyses, performed on the Quickmag recordings of the fingertip, with the power law analyses performed on the low-noise robot endpoint trajectories calculated from the joint angles, the filter cutoffs applied to the vision-based recordings were adjusted to obtain a maximal matching of the data.

Joint angle reconstruction

The six measured markers allowed an analytically well-defined reconstruction of the joint trajectories of the subjects, employing the biomechanically derived coordinate system of Wood et al. (1989). Figure 1 shows this coordinate system. Based on the finding that

[2] In a pilot study, three subjects executed the same set of elliptical movement patterns with the one difference that they were not asked to close their eyes. While the results on the main dependent measures did not differ from the ones of the reported experiment, the subjects reported a tendency to orient their patterns toward objects in the laboratory, i.e., walls, closets, or other planar objects. To avoid any interference from such external influences, we opted to instruct them to close their eyes.

cyclic drawing patterns are produced by approximately sinusoidal oscillations in joint space (Buchanan et al. 1997; Guzman et al. 1997; Soechting and Terzuolo 1986; Soechting et al. 1986), the seven joint angle trajectories were fitted with sinusoids. The fundamental frequency of each pattern was determined from the fundamental peak of the FFT analysis of the endpoint trajectory. Since the patterns were performed stably over the 15-s trials, this fundamental frequency f must coincide with the fundamental frequency of each DOF. Given the fundamental frequency, the amplitudes and phases of the sinusoidal fits of the joint trajectories were approximated by a linear regression of the coefficients a_0, a_1, and a_2 of the equation $\theta(t)=a_0+a_1\sin\omega t+a_2\cos\omega t$, where $\omega=2\pi f$. The amplitude and phase of each DOF can be determined from these coefficients as $A=\sqrt{a_1^2+a_2^2}$ and $\varphi=\arctan(a_1/a_2)$.

Consequently, a complete approximation of each trial was obtained in terms of sinusoidal joint motion, together with a coefficient of determination indicating the quality of fit of each sinusoid.

Descriptive measures of the endpoint trajectory

Frequency. The mean period or frequency of one trial was computed from the fundamental frequency of the fast Fourier transform (FFT) analysis of the endpoint trajectory.

Perimeter. To quantify the pattern size, the mean perimeter of each ellipse was computed by summing over the Euclidean distances of subsequent data points and dividing by the number of elliptical cycles per trial. The number of repeated cycles was obtained from the fundamental frequency of the FFT analysis of each pattern and the trial duration.

Planarity. The planarity of the elliptical patterns was defined as the magnitude of the movement orthogonal to the major and minor axes of the elliptical pattern, thus quantifying the ellipse's deviation from its two-dimensional (2D) extent. Therefore, large values of planarity corresponded to large deviations from the 2D extent. For this calculation, the patterns were first split into trajectory pieces of one-period duration. Second, the covariance matrix and its eigenvalues were determined for each trajectory piece using the x, y, and z values of all sampled data points of the segment. Third, the square root of the smallest eigenvalue captures the deviation from strictly 2D performance. Finally, the planarity estimate of one trial was obtained from the mean over all single-cycle values. Performing the calculations on a cycle-by-cycle basis was necessary to avoid noise effects from slow drifts in the subjects' performance. Although the smallest eigenvalue is generally vulnerable to noise, the calculated values from the present data set nevertheless provide a reliable indicator for planarity (for more details, see Sternad and Schaal 1999).

Power law exponent. The radius of curvature and the tangential velocity of the elliptical patterns were calculated according to the standard formulae in Eq. 1. More critical were the estimations of the velocity gain factor k and the exponent β of the power law. Two different methods were used. First we followed the typical procedure of determining the exponent from a log-log regression (Lacquaniti et al. 1983). While this is a common analysis technique for extracting exponential coefficients, there is an important statistical issue to be considered, especially when the exact magnitude of the linearized fit of the exponent is important. A regression on the log-log data is inherently biased, since it de-emphasizes the error of data points at the higher values of the variables (see also Elzinga 1985). In the present case, it underestimates errors at higher tangential velocities. This can be readily appreciated when one compares the cost functions for the nonlinear regression with the one for the log-log regression; while in the nonlinear case the cost function $J_{nonlinear}$ is the regular squared deviation between predicted $\hat{v}_i$ and actual tangential velocities v_i:

$$J_{nonlinear}=\frac{1}{2}\sum_{i=1}^{N}(v_i-(kr_i^{\beta}))^2=\frac{1}{2}\sum_{i=1}^{N}(v_i-\hat{v}_i)^2 \qquad (2)$$

the log-log regression minimizes a cost J_{log} using the ratio of v_i and $\hat{v}_i$:

$$J_{\log}=\frac{1}{2}\sum_{i=1}^{N}(\log v_i-(\log k+\beta\log r))^2=\frac{1}{2}\sum_{i=1}^{N}\left(\log\frac{v_i}{kr_i^{\beta}}\right)^2 =\frac{1}{2}\sum_{i=1}^{N}\left(\log\frac{v_i}{\hat{v}_i}\right)^2 \qquad (3)$$

where N denotes the number of data points in one trial.

To minimize J_{log}, $v/\hat{v}$ is optimized toward 1, where the log function equals zero. This means that for larger v a larger error in $\hat{v}$ will be tolerated, since it is not the absolute error, as in Eq. 2, but rather the relative error that is minimized. Conversely, for small v, only an unproportionally small error in $\hat{v}$ will be tolerated. Statistically, minimization of Eq. 3 assumes that the data have an error component that is log-normally distributed, i.e., the smaller the v, the smaller the error and vice versa. From our point of view, it is unclear whether this assumption is justified for power law data: for instance, some results in the literature argue in favor of increasing variance with increasing force production (Newell and Carlton 1988), while others report more variability in low-velocity regions of the trajectory (Haggard and Richardson 1996). For this reason, we also analyzed the untransformed data directly by using the nonlinear Levenberg-Marquardt least-squares regression (Press et al. 1989). In the Results section, we demonstrate that the two different data analysis techniques can have a profound impact on the quality of fit of the power law.

Data modeling and robot implementation

In order to replicate the human data with the anthropomorphic robot, the ten trials of each subject from one set of different-sized patterns were sorted according to their mean perimeters. For each joint angle θ_i, a weighted regression analysis was performed (Myers 1990), regressing each of the three parameters of the sinusoid, i.e., frequency f, amplitude A, phase, against the perimeter p, thus resulting in:

$$\theta_i(t,p)=A(p)\sin(2\pi f(p)t+\varphi(p)),\quad \text{where}$$
$$A(p)=d_0+d_1p$$
$$f(p)=b_0+b_1p$$
$$\varphi(p)=c_0+c_1p$$

where d_0, d_1, b_0, b_1, c_0, and c_1 are the linear regression parameters. Using weighted regression analyses was necessary because the parameters of the sinusoidal fits for the different-sized joint trajectories had different variances. A nonweighted regression over such data would violate the linear regression model that assumes equal variance in all data points. Weighted regression multiplies the input and output of each data point i with a weight $w_i=1/s_i$, where s_i is the standard deviation of the ith data point (Schaal and Atkeson 1998). After this transformation, the regression analysis proceeds as usual. In the present case, since the true standard deviations of the sinusoidal-fit parameters are not easily obtained from the non linear equations for $A=\sqrt{a_1^2+a_2^2}$ and $\varphi=\arctan(a_1/a_2)$ (see section Joint angle reconstruction), we used the square root of the coefficient of determination of the sinusoidal fit as a weight, i.e., $w_i=\sqrt{R_i^2}$, assuming that it approximately reflects the reciprocal of the standard deviation of the coefficients of the sinusoidal fits. Thus, the weighted regression de-emphasized the influence of data points stemming from sinusoidal fits with low coefficients of determination.

As a result of these regressions, we obtained linear scaling relations of how the joint angle motions, i.e., their frequency, amplitude, and phasing, varied as a function of the pattern size. From these scaling relations, we chose five sets of parameters to generate the desired joint positions, velocities, and accelerations for five pattern sizes for every subject in every experimental condition. The five parameter sets were picked equidistant between the values for the smallest and the largest perimeter (see also Results). This kinematic description of joint motion sufficed to repeat the patterns with the anthropomorphic robot arm by using it as desired trajectory input for an inverse model in conjunction with a PD

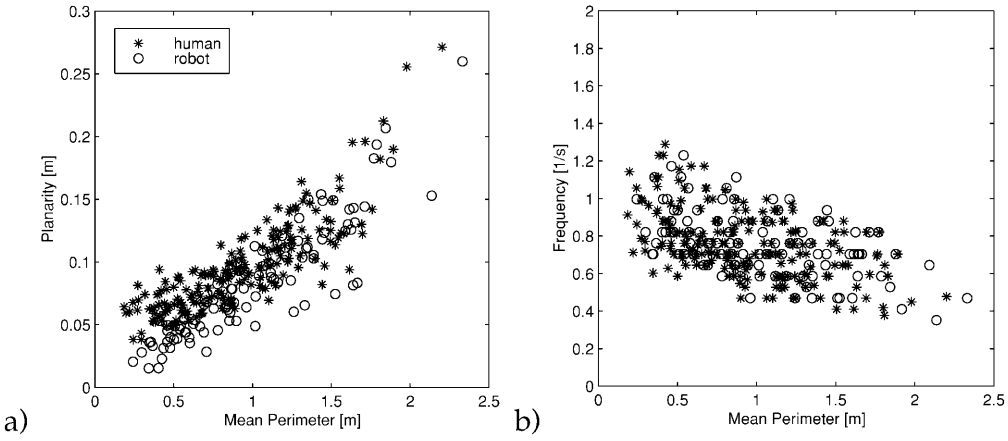

Fig. 2a,b Kinematic descriptors obtained for all trials in human (asterisks) and robot (circles) data. **a** Planarity per trial versus mean perimeter. **b** Mean frequency per trial versus mean perimeter

controller. We recorded the Cartesian fingertip movement of the robot with the Quickmag vision system for 15 s for each movement pattern. Thus, the pattern realized by the robot could be analyzed in the same way as the human data.

Results

Human data

Descriptive measures

A first set of analyses extracted the relevant kinematic variables to describe the subjects' performance across the experimental conditions. In accordance with the instructions, subjects traced ellipses over a large range of different sizes, yielding an approximately uniform distribution of mean perimeters ranging between 0.21 and 2.23 m. Typical realizations of such patterns were shown in previous work (Sternad and Schaal 1999). In general, subjects traced proper elliptical patterns in the smaller-size conditions, while for some workspace locations the large patterns show distortions from elliptical (for an explanation, see Sternad and Schaal 1999). Figure 2a plots the measure of planarity as a function of the mean perimeter of each trial. With increasing pattern size, the planarity measure increased, indicating that large ellipses increasingly deviated from a strictly planar shape, i.e., had a significant 3D structure. Figure 2b shows the temporal dependency of the elliptical patterns on the mean perimeter. In all subjects, the mean frequency of the elliptical patterns decreased with increasing pattern size, but it decreased much more slowly than the mean perimeter increased. Similar observations have been reported in previous studies (Viviani and Cenzato 1985; Viviani and Flash 1995; Viviani and Schneider 1991).

Power law fits

The endpoint trajectories of human data were used to determine the coefficients of the power law. Figure 3a–d shows the results of the power law fits for one representative subject performing the four different pattern orientations. Each panel shows the results for the β coefficients of ten trials, estimated with the nonlinear regression (see Materials and methods) and graphed as a function of the mean perimeter of each trial. To illustrate the quality of the power law fit, the coefficients of "nondetermination" ($1–R^2$) are included to provide a "confidence band" of $\pm 0.5\times(1–R^2)$ around the β-values. It is important to note that these "confidence bands" are *not* a confidence measure of each β-value, but rather a confidence measure of the entire power law fit. Thus, Fig. 3 superimposes two quantities in one graph to allow inspection of the quality of the power law fits at one glance.[3]

Figure 3a shows the "confidence points" for each trial with "+" signs, while in the other charts they were omitted for reasons of clarity. In order to capture the trend of the power law fits as a function of pattern size, we fitted polynomials of maximally second order to the β-values and the R^2-values by using a stepwise regression, thus obtaining β- and R^2-values as functions of the perimeter p:

$$\beta=a_0+a_1p+a_2p^2 \quad \text{and} \quad R^2=b_0+b_1p+b_2p^2 \tag{4}$$

The results of these regressions are added as solid lines in Fig. 3 to depict the trends of the data more clearly. Using a stepwise regression ensured that all fits of the trends in Eq. 4 were significant at a level of $P<0.05$. Across all subjects and conditions, we obtained 20 such fits of the parameter trends (one for each condition for each subject). Of these 20 fits, 18 had a significant linear or quadratic trend in the β-values. In the two cases where the stepwise regression favored a constant fit, there was

[3] Using a Bayesian nonlinear regression procedure, we also calculated the confidence bands on the β-values. Across all subjects and conditions, these confidence bands were very narrow, and they are not recognizable in Fig. 3. Also, the confidence bands of the β-values are not relevant to our analysis: the confidence band on a regression parameter can be very narrow even if the regression analysis is not significant. The confidence band of the regression parameters is typically determined by the leverage that the data provide to determine the parameters accurately, while the quality of the regression is determined by the suitability of the model that was fitted to the data. The latter point is what we pursue in our analyses: a statement about the suitability of the power law model for rhythmic movement generation.

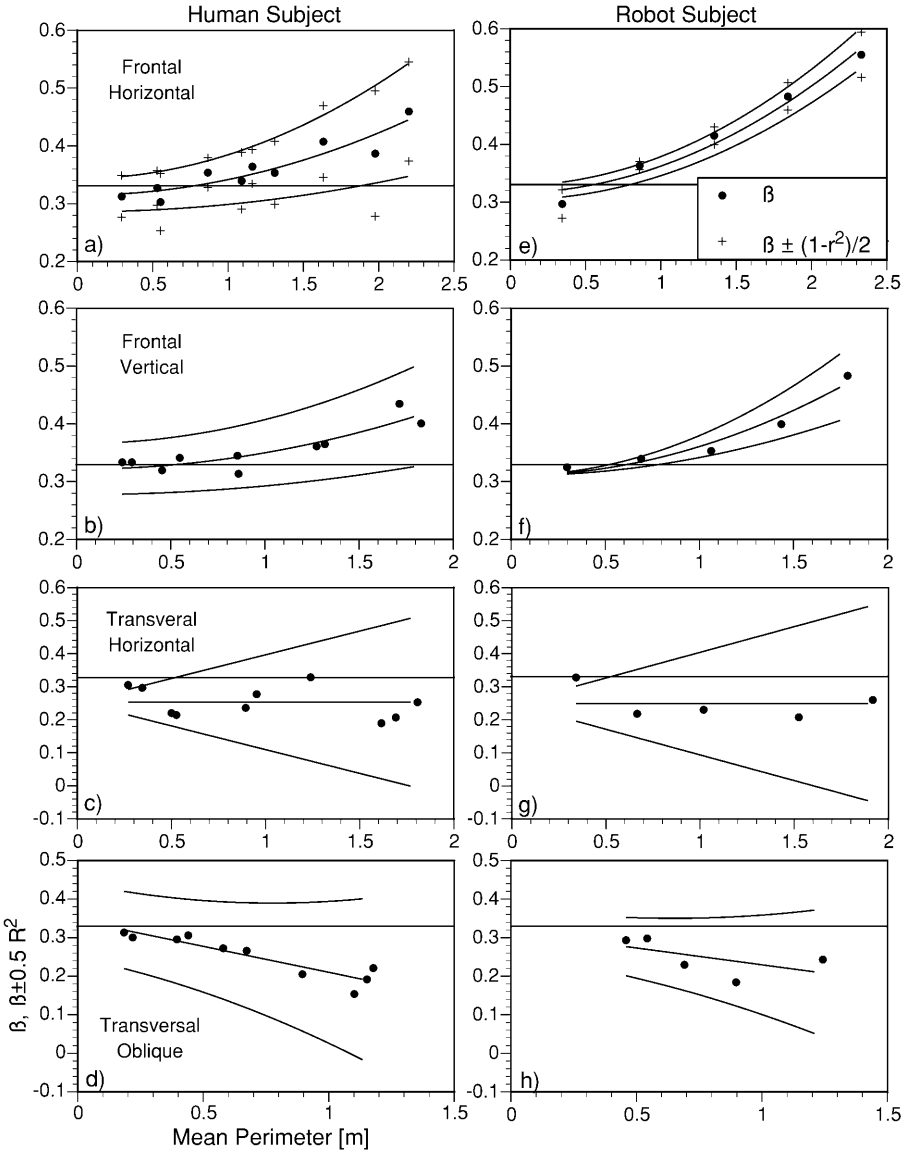

Fig. 3a–h Estimates of the coefficient β of the power law as a function of the mean perimeter of each trial. To indicate the quality of the regressions, a "confidence band" of $\beta \pm 0.5 \times (1-R^2)$ is added in each graph. The data points of β and R^2 were interpolated by polynomial regressions to visualize the trend of the data. For comparison the *dimmed horizontal line* indicates the power law coefficient β=1/3. **a–d** Data from one human subject in the four different experimental conditions; **e–h** the corresponding robot results

a significant deviation of the β-values from the target value of 1/3 (tested by *t*-tests with a 0.05 significance level). Additionally, 13 out of 20 fits had a significant linear or quadratic trend in the R^2-values. These trends are statistical evidence that the size variations of the elliptical patterns had a significant impact on the quality of the power law fits.

As a summary result of the power law fits across all subjects and experimental conditions, two main observations can be discerned: for small pattern sizes, the power law coefficient β is close to the expected 1/3, for larger pattern sizes, however, the fit continuously degrades. This degradation is indicated as either an increasing deviation from the target value 1/3, or an increasingly worse fit of the power law coefficients, i.e., lower R^2-values expressed in the widening of the confidence band in Fig. 3. It should be emphasized that the degradation of the power law fits is often so severe, e.g., on the order of 30–40% difference from the original value 1/3, that it is not possible to dismiss it as a tolerable variation of an empirically determined law of human movement coordination.

Power law fits: log-log or nonlinear regression?

In the Materials and methods section, we mentioned that our data analyses employed nonlinear regression techniques to extract the coefficients of the power law, while most previous investigations made use of log-log regressions. Appendix A provides empirical evidence that the log-log regression systematically *underestimates* the absolute deviations from the coefficient 1/3, such that care must be taken in interpreting the absolute values of previous power law studies that employed log-log regressions. However, the trend of degradation of the power law with larger patterns size remains the same in both analysis techniques.

Table 1 Median and interquartile range of R^2-values of sinusoidal fits binned into 0.1-rad intervals of the amplitude of the angular motion. The interquartile range gives the distance between the lower and upper quartile and represents a robust statistic for the standard deviation (Huber 1981)

R^2	Amplitude range (rad)						
	0.0–0.1	0.1–0.2	0.2–0.3	0.3–0.4	0.4–0.5	0.5–0.6	0.6–0.7
Median	0.62	0.83	0.86	0.87	0.91	0.96	0.86
Interquartile range	0.38	0.21	0.15	0.14	0.14	0.08	0.17

Joint angle trajectories

In addition to the analysis of the endpoint trajectories, we further investigated the joint angle trajectories of the human subjects that generated the endpoint trajectories. Similar to previous results obtained by Soechting and Terzuolo (1986) and Buchanan et al. (1997), all time series of the seven joint angles were sufficiently regular to allow their fitting by sinusoids. Table 1 lists the R^2-values across all subjects in the four pattern orientations. To better reflect the dependency of the R^2-values on the joint angular amplitudes, the R^2-values were binned according to amplitude ranges. For each bin, the median and interquartile range is shown as a robust statistic for the mean and the standard deviation. Robust statistics had to be used in this case because the distribution of R^2-values in each bin deviated significantly from a normal distribution.

Except for very small joint angular amplitudes, the R^2-values of sinusoidal fits were always highly significant, expressed by R^2-values greater than 0.8. The fact that larger joint angle amplitudes have higher R^2-values is largely due to our recording technique: Since the markers attached to the subjects' arms are necessarily offset from the neutral axis of the joint, even single-DOF movement can cause displacements in several markers which will be interpreted as if several DOFs were moving. This spurious movement reduces the signal-to-noise ratio, particularly for small angular amplitudes. In some trials, a slow drift in frequency also contributed to a reduction of the R^2, although the pattern was otherwise approximately sinusoidal. Despite these data contaminations, it was always possible to faithfully reproduce the main effects of the human movement with the sinusoidal model, as subsequent results will demonstrate. Apart from the observation that the angular motions of wrist supination-pronation (WSP), wrist flexion-extension (WFE), and wrist adduction-abduction (WAA; see Fig. 1) had generally lower amplitudes, we could not find any particular preference in subjects as to which DOFs contributed most to the patterns. A more detailed discussion of how to generate joint angle trajectories from marker data can be found in previous work (Sternad and Schaal 1999).

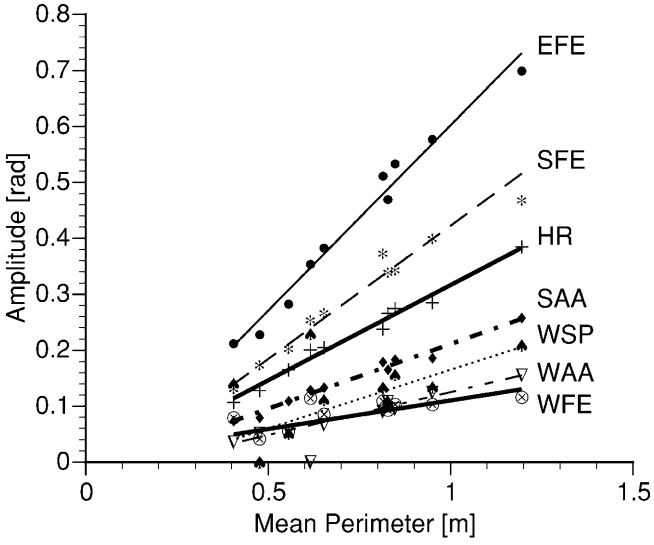

Fig. 4 Representative set of amplitudes of the seven joint angles versus their corresponding mean perimeter from one subject performing a block of trials in the transversal-oblique pattern orientation

Data modeling and robot implementation

After fitting the amplitude, frequency, and phase parameters for each DOF of each experimental trial, one more step was performed before the modeled data were implemented on the robot arm. To avoid an exact replication of each trial but rather to implement a subject's generic drawing strategy, the sinusoidal parameter sets across all pattern sizes were interpolated by linear regression for each subject. Figure 4 shows the amplitude values and regression lines obtained from one representative subject as a function of the mean perimeter. The linear scaling in Fig. 4 was observed in all subjects. The phase differences between joint oscillations were determined pairwise between the shoulder angle and the six other DOFs, respectively. Importantly, the pairwise phase differences did not change across the different pattern sizes: out of a total of 140 linear regressions for the phase offset as a function of the perimeter (7 DOFs × 4 conditions × 5 subjects), only four linear fits showed a statistically significant linear trend ($P<0.05$). The scaling of the frequency as a function of the mean perimeter is presented in Fig. 2b.

The modeled set of joint trajectories of the human data were implemented on the robot arm, which then "mimicked" each of the five subjects. It is important to emphasize that the endpoint trajectories of the robot were recorded and processed in exactly the same way as the human data, yielding an analogous set of dependent

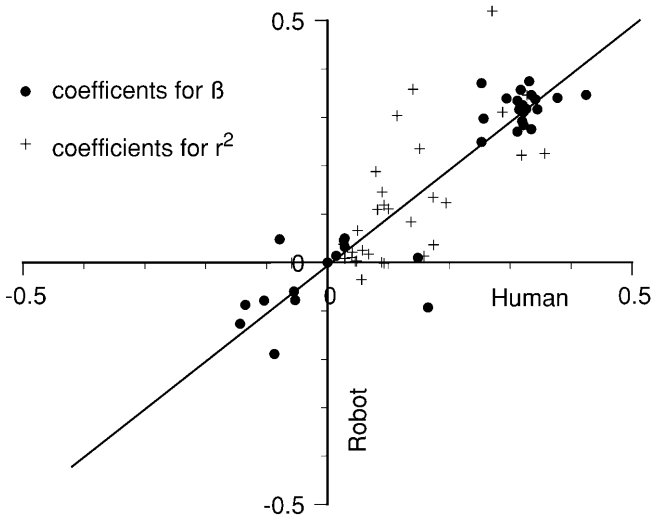

Fig. 5 Comparison of the coefficients of the polynomial regressions capturing the trends of the power law fits in human and robot data (cf. Fig. 3). Each data point is composed from a polynomial coefficient from human data on the horizontal axis and the corresponding robot coefficient on the vertical axis. Constant, linear, and quadratic coefficients across all subjects and all conditions are pooled

variables with the same kind of measurement noise. The measures of mean perimeter, planarity, and mean frequency of the robot's ellipses performed at five pattern sizes were calculated. The results are shown in Fig. 2 superimposed on the human data. There is hardly any visible difference between the human data and the robot data, except that the robot data show slightly smaller values of planarity, since this measure captures to some extent the variability of the experimental patterns.

Power law fits

Figure 3e–h depicts the results of the power law fits when the robot mimicked the patterns of the subject displayed in Fig. 3a–d. There is a remarkable similarity between the trends of the β coefficients between the robot and the human data. As in the human data, for small perimeter values, β=1/3 was produced quite accurately, but, as in the human subjects, the same deterioration of the power law fits were apparent for increasing pattern size. The similarity of the trends of the human and robot data is summarized in Fig. 5. To generate this graph, we plotted the coefficients of the polynomial fits for the trends of the β and the R^2-values of the robot versus the corresponding coefficients from the human subjects (cf. Eq. 4). For every subject and every experimental condition, we obtained a set of polynomial coefficients, $a_0^h, a_1^h, a_2^h, b_0^h, b_1^h, b_2^h,$ for the human subject and the corresponding $a_0^r, a_1^r, a_2^r, b_0^r, b_1^r, b_2^r,$ for the robot. Figure 5 plots these coefficients pooled across all subjects and all conditions in a pairwise fashion as $(a_0^h, a_0^r), (a_1^h, a_1^r), (a_2^h, a_2^r)$ $(b_0^h, b_0^r), (b_1^h, b_1^r), (b_2^h, b_2^r)$. The clustering of the degrading power law fits around the identity line confirms that the robot data generated power law fits with the same main features as the human data.

Discussion

With the goal of investigating the generative mechanisms of rhythmic arm movements, the present experiment tested the validity of the 2/3 power law in unconstrained arm movements where subjects performed large-scale elliptical patterns in three dimensions involving the whole arm. Elliptical patterns were chosen because they are the simplest rhythmic traces, and small ellipses drawn in two dimensions have been repeatedly analyzed in the literature on the power law. Patterns of ten different sizes were performed by five human subjects in three different areas of the workspace. Each trial was analyzed in terms of the trajecotry of the fingertip and the arm's seven joint-angle trajectories that were involved in the pattern realization. By modeling the joint angle trajectories with simple sinusoidal fits, we could replicate the subjects' movements on a 7-DOF anthropomorphic robot arm. Comparative analyses of the endpoint trajectories of human and robot performance converged to one common result: while for small pattern sizes the power law was satisfied accurately, it was increasingly compromised for larger patterns, where up to 30–40% difference from the coefficients of the original law were observed. Therefore we concluded that the power law was an unlikely candidate for explaining rhythmic movement generation in human motor control.

At first glance, one may suspect that the observed deviations from the power law could be due to an incorrect extraction of the relation between velocity and curvature. Viviani and Cenzato (1985) have already emphasized that the power law is only valid within appropriately defined movement segments. This point was the subject of a previous study that addressed the issue of segmentation in similar elliptical patterns to those in the present experiment (Sternad and Schaal 1999). Their results gave strong evidence against the hypothesis that elliptical patterns are composed of multiple movement segments and dismissed several criteria that had been previously suggested to delineate movement segments. Thus, it is necessary to resort to another line of argument to account for our findings. In the following, we will develop an argument that the power law is an epiphenomenon of smooth, oscillatory trajectory generation in joint space, at least for unconstrained rhythmic movement.

The power law as an expression of smoothness

Our first and major hypothesis is that the power law is effectively an expression of smoothness of endpoint trajectories. A similar argument was presented by Todorov and Jordan (1998), however, with the difference that

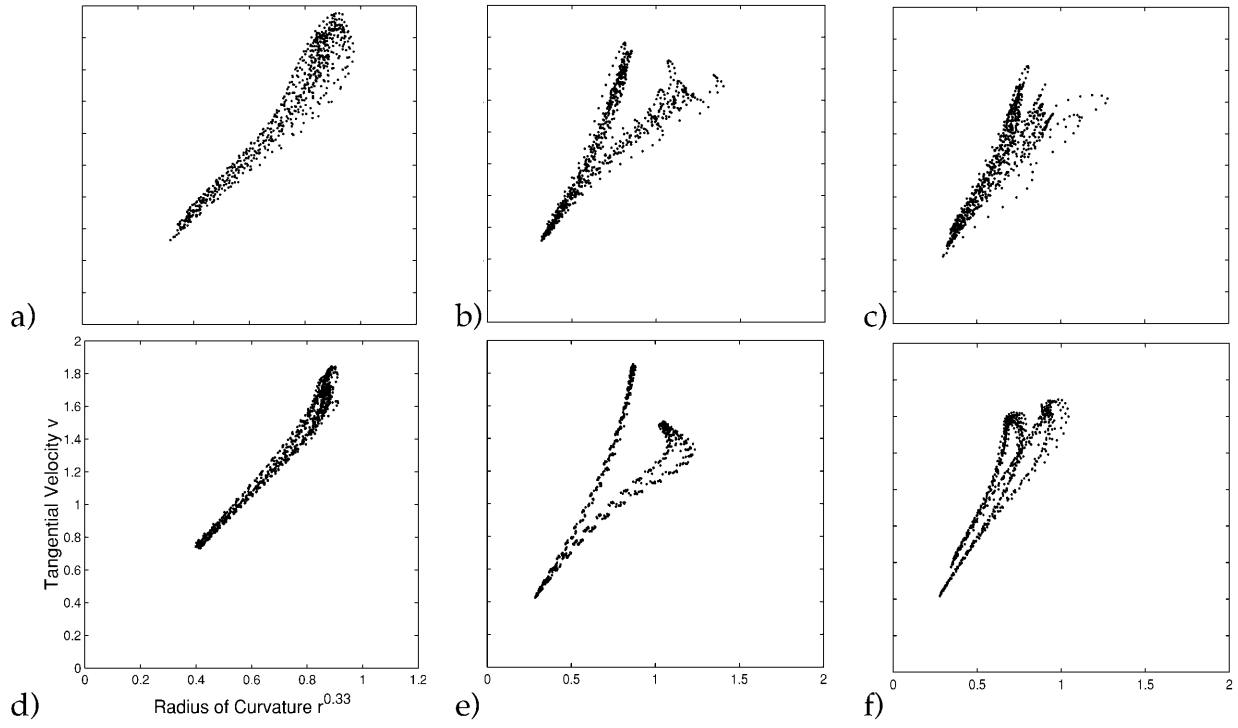

Fig. 6a–f Tangential velocity versus radius of curvature to the power 1/3 for three typical cases of power law degradation. **a–c** Human trials; **d–f** corresponding robot trials

their experiments addressed the tracing of discrete paths in two dimensions and three dimensions, and modeled them using a complex optimization criterion, the constrained minimum jerk. As will be shown in the following, a simpler smoothness criterion can account for our data.

For the purposes of our argument, smoothness is defined as low power in the higher-frequency components of the endpoint trajectory. For example, a harmonic oscillation is maximally smooth and is equivalent to a rhythmic minimum jerk trajectory. There exists a tight connection between the power law and harmonic oscillations: in a Lissajous plot, two or three orthogonally arranged sinusoids with a phase offset trace out a planar ellipse whose velocity-curvature relation satisfies the power law exactly (Lacquaniti et al. 1983; Morasso 1983; Soechting and Terzuolo 1986). Evidently, both the power law and minimum jerk model are equally fulfilled in this case, a fact that also hints at a close connection between minimum jerk and the power law (Todorov and Jordan 1998; Viviani and Flash 1995). Next we will discuss the power law as a definition of smoothness in the context of our data.

After Lacquaniti et al. (1983), an alternative method to visualize the realization of the power law in the data is to plot tangential velocity v against the radius of curvature r raised to the power 1/3 (referred to as v-r plot). This way of graphing assumes that the exponential relation is satisfied and thereby affords inspection of the time course of the parameter k throughout the periodic pattern. If the power law is satisfied, the velocity gain factor is constant and the data lie on a straight line through the origin; the slope of the line expresses the velocity gain factor k. Figure 6 shows v-r plots for three exemplary large-size patterns. Clearly, the power law is violated throughout the rhythmic trace in a systematic fashion. Figure 6a is typical for patterns in the frontal plane, Fig. 6b is primarily observed in horizontal ellipses in the transversal plane, and Fig. 6c is common in transversal oblique patterns. Figure 6d–f depicts the corresponding robot trials. Importantly, the robot, although explicitly driven by joint-space sinusoids alone, reproduces strikingly similar distortion features to found in the human subjects.[4] Applying our smoothness criterion, we can explain how these complex structures arise. A discussion of how such distortions affect the 3D realization of the elliptical patterns as well as a geometric interpretation for these distortions has already been presented in previous work (Sternad and Schaal 1999).

If the power law, as expressed in Eq. 1, is an explicit constraint in the CNS for the generation of rhythmic movement trajectories in Cartesian space, there are two alternatives for its implementation: (1) the power law relation is somehow implemented directly in the neural substrate, i.e., some set of neurons realize Eq. 1 and are used in movement planning; or (2) the power law is implemented indirectly. The latter can be achieved by maximizing the smoothness of Cartesian trajectories, equivalent to minimizing higher-frequency components of the

[4] It is also noteworthy that the deviation of the data from a straight line happens in the high-velocity areas, exactly those areas that would be de-emphasized by log-log regressions of the power law coefficients (see Appendix A).

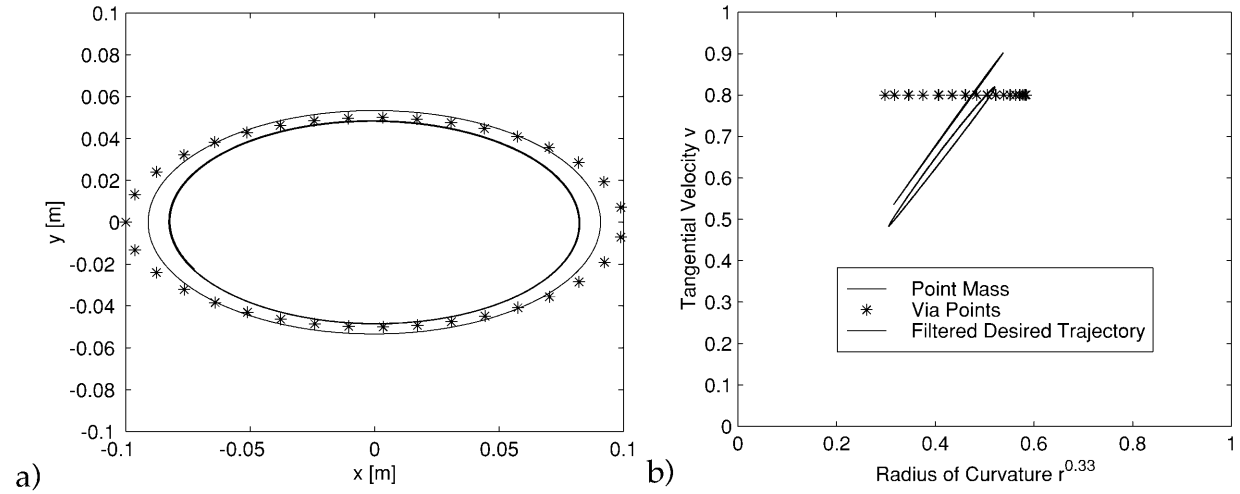

Fig. 7 **a** Desired and realized elliptical trajectories for point mass and Butterworth filter. *Stars*, via points; *bold solid line*, path traced out by the point mass; *thin solid line*, smoothed trajectory. **b** *v-r* plots corresponding to the trajectories in **a**

endpoint trajectory or to minimizing jerk. Such a process automatically leads to trajectories that conform with the power law, as mentioned above. However, since our data demonstrate a deviation from the power law for large patterns, neither of these solutions seems to be used by our subjects.

Yet, why are there so many studies that show that the power law is obeyed, including our results for small patterns? As laid out formally in Appendix B, it is possible to reconcile all observations about the power law if, for rhythmic movements, smoothness is implemented in intrinsic, e.g., joint space, coordinates. For small patterns, smoothness in intrinsic coordinates is equivalent to smoothness in Cartesian coordinates, because the transformation between joint coordinates and extrinsic endpoint coordinates is approximately linear. Thus, the power law will be satisfied for small patterns. For larger patterns, smoothness in joint coordinates no longer results in smoothness in extrinsic coordinates as the nonlinearities added by the kinematic transformation become increasingly larger. It is these nonlinearities that cause deviations from the power law. The relevance and primary contribution of joint space trajectories to endpoint movements is supported by the fact that joint trajectories can be fitted with high significance by simple sinusoids that subsequently capture the major features of human data. Further, the linear scaling of the amplitudes of the joint space sinusoids as a function of pattern size (Fig. 4) indicate the primary role of joint space in movement generation.

The 2/3 power law as by-product of smooth trajectories

Taken together, the above arguments make it unlikely that the power law – a law relating the geometric path and the timing of the *end-effector* trajectory – is a first-order criterion for the generation of rhythmic movements. Rather, we agree with Todorov and Jordan (1998) that it seems to be a by-product of smooth trajectories. Smoothness is a topic that has been predominant in many approaches to motor control (Flash and Hogan 1985; Todorov and Jordan 1998; Uno et al. 1989; Viviani and Flash 1995; Viviani and Schneider 1991). Yet whether smoothness is implemented in intrinsic or extrinsic coordinates and whether based on kinematic or dynamic criteria remains a topic of current research (Harris and Wolpert 1998). Our suggestion that unconstrained rhythmic movement favors smoothness in joint space is in agreement with previous work. Smoothness in joint space corresponds to minimum jerk movements in joint space, which is a first-order approximation to the minimum torque change criterion, as long as the movement is not too fast (Uno et al. 1989). Despite this correspondence, caution is necessary in generalizing our results to discrete movements. Rhythmic and discrete movement may not share the same movement-generating principles – after all, rhythmic movement is phylogenetically older than discrete movement and could employ different neural circuits.

Returning to the discussion of smoothness in the context of the power law, it can be shown nicely how directly a smoothness criterion can lead to the generation of the power law. In simulating movements with a two-joint arm using the λ-version of the equilibrium point hypothesis, Gribble and Ostry (1996) argued that limb dynamics, muscle mechanics, and physiology contribute significantly to producing the power law. Although their planned or virtual trajectory consisted of 36 via points traversed at a *constant speed* across an elliptical path, the actual trajectory realized by the simulation satisfied the power law. What the authors effectively demonstrated is that the arm, muscle, and λ-dynamics have one common effect: they act as low-pass filters. Low-pass filtering takes away higher frequency components in the resulting movement, i.e., it increases smoothness. As demonstrated in Appendix B, a strong enough filter will cause the power law to emerge.

To demonstrate that this effect does not require the simulation of a complex, biomechanically validated arm, we repeated Gribble and Ostry's (1996) experiment in a highly simplified way. A 0.6-s periodic movement was generated using 36 via points with equal distance in time and space along the perimeter of a planar ellipse with a 0.2-m major axis and a 0.1-m minor axis. These measurements exactly replicated Gribble and Ostry's (1996) parameters. By linearly interpolating between these via points, we generated a desired trajectory for a simulated point mass of 1 kg weight for a 500-Hz control loop; the linear interpolation resembles the constant velocity shifts of the λ-trajectories. The point mass was controlled to stay on the desired trajectory with a PD controller, using a proportional gain of 50 and a velocity gain of 5. Note that the *desired* velocity along the trajectory was assumed to be zero, hence realizing a pure damping term. Thus, we effectively used a *constant* tangential velocity trajectory as the tracking input for an elliptical path. Figure 7a shows the results of this simulation, illustrating the via points together with the path traced out by the point mass. As shown by Gribble and Ostry (1996), the trajectory realized by the controller had a smaller perimeter than the desired trajectory; our PD gains were chosen to quantitatively reproduce this scaling. Figure 7b depicts the corresponding *v-r* plots: while the via-point trajectory does not obey the power law (the slope is zero and does not pass through the origin), the point mass's trajectory achieves an exponent β=0.327, i.e., an almost perfect power law fit.

Yet, the same effect can be achieved in an even more straightforward way: we simply passed the desired trajectory through a fourth-order Butterworth filter with 2.5-Hz cutoff frequency. These results are also presented in Fig. 7 by the thin solid line. The power law fit for this smoothed trajectory was β=0.328.

We conclude that any kind of mechanism that generates smooth, rhythmic trajectories is likely to display the phenomenon of the power law. This, however, does not imply that the power law is directly used as a movement-generating principle. By investigating different pattern and workspace conditions, we demonstrated that the power law is systematically influenced by such conditions, showing that it is not a primary factor in movement generation. For unconstrained rhythmic movement, smooth oscillatory pattern generators in joint space seem to be the most parsimonious explanation for all observed movement features, including the power law.

Acknowledgements Frank Pollick's and Nicolas Schweighofer's comments on an earlier version of this manuscript contributed significant improvements. This work was made possible by grant 9710312 of the National Science Foundation, the ERATO Kawato Dynamic Brain Project, funded by the Japanese Science and Technology Cooperation, and the ATR Human Information Processing Research Laboratories.

Appendix A: log-log or nonlinear regression for power law fits?

In the Materials and methods section, we indicated a potential problem when extracting exponents from log-log transformed data and showed that there are significant statistical differences between a regression on untransformed and on double-logged data. In a log-log regression, errors associated with higher tangential velocities are underestimated, or, alternatively, the assumption about a log-normal distribution of errors needs to be satisfied. This assumption has never been validated for power law studies, and contrasting results have been published on the variability of endpoint trajectories (Haggard and Richardson 1996; Newell and Carlton 1988). Thus, applying a log-log regression carries the potential danger of distorting the power law fit results.

Given that the long series of studies on the power law exclusively used the log-log method, it is worthwhile to examine the kind of bias introduced by such regressions. Figure 8 compares the results of the two different fitting methods applied to the trials of one experimental condition, which is depicted in Fig. 3d. The two fitting methods result in clearly different estimates for both the power law coefficient and the coefficient of determination of the regression. While the trend of degradation of the power law fit as a function of perimeter is preserved in both fitting methods, it is apparent that in Fig. 8b the linear log-log regression generates coefficients β that lie closer to the "desired" value 1/3. Further, the R^2-values of the fit are generally larger such that the band delineated by the coefficient of nondetermination $1–R^2$ is narrower.

To demonstrate that this exemplary trend toward a better power law fit is not a singular result, we quantified the bias for all trials and subjects and calculated the mean difference between nonlinear and log-log regressions as $\Delta\beta=|\beta_{nonlinear}–1/3|–|\beta_{\log}–1/3|$ and $\Delta R^2 = R^2_{nonlinear} - R^2_{\log}$. Note that Δβ uses the *absolute* deviation from the ideal value 1/3 such that it can directly serve to compare the statistical bias in both regression techniques. As Fig. 9 summarizes, Δβ is positive for the four experimental pattern orientations, implying that the log-log regression consistently produces a result that is biased toward the value 1/3. This is accompanied by a higher R^2 of the log-log regression, recognizable from the consistently negative mean values of ΔR^2. All mean values of Δβ and ΔR^2 in Fig. 9 are significantly different from zero, according to a two-tailed *t*-test ($P<0.05$). Thus, in both statistics the log-log regres-

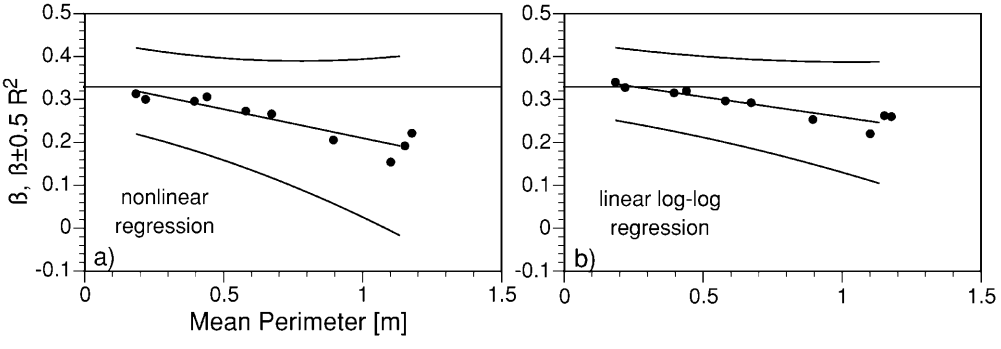

Fig. 8a,b Power law fits for the trials of the experimental condition from Fig. 3d (see legend to Fig. 3 for explanations of the plots), **a** using nonlinear Levenberg-Marquardt regression; **b** using linear log-log regression

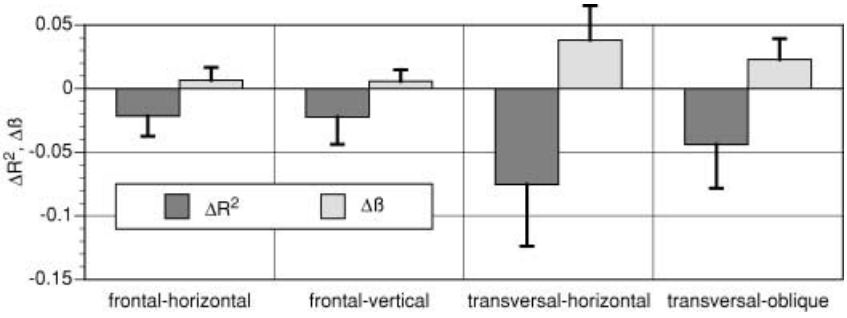

Fig. 9 Power law fits of human data contrasting the results of nonlinear and log-log regression. Categorized by experimental condition, the bars show the mean and standard deviations of the differences in β- and R^2-values, defined as: $\Delta R^2 = R^2_{nonlinear} - R^2_{\log}$ and $\Delta\beta = |\beta_{nonlinear}–1/3|–|\beta_{\log}–1/3|$

sion is biased toward a better fit of the power law and is thus likely to favor too optimistic interpretations of power law data.

Appendix B: the relation between power law and smoothness

Assume β=1/3 (as is done in the *v*-*r* plots) and solve Eq. 1 for the velocity gain factor *k*, then the following equation is obtained:

$$k(t) = \frac{v(t)}{r(t)^{1/3}} = v(t)c(t)^{1/3} = \|\dot{\mathbf{x}}(t) \times \ddot{\mathbf{x}}(t)\|^{1/3} \tag{B1}$$

The expression on the right is obtained by substituting all variables according to the definitions in Eq. 1. Note that *k* is now written as a time-varying quantity, and the following analysis will discuss the temporal dependence of *k* as an alternative way to explore conditions when the power law is achieved.

Since the experimental test patterns are periodic, it is possible to represent the endpoint trajectory $\mathbf{x}(t)$ by a finite Fourier series of the order *n*:

$$\mathbf{x}(t) = \begin{pmatrix} x(t) \\ y(t) \\ z(t) \end{pmatrix} = \begin{pmatrix} \sum_n a_{x,n} \sin(n\omega t + \varphi_{x,n}) \\ \sum_n a_{y,n} \sin(n\omega t + \varphi_{y,n}) \\ \sum_n a_{z,n} \sin(n\omega t + \varphi_{z,n}) \end{pmatrix} \tag{B2}$$

After differentiation with respect to time to obtain velocities and accelerations, Eq. B1 can be rewritten for the general case of 3D periodic patterns:

$$k(t) = \|\dot{\mathbf{x}}(t) \times \ddot{\mathbf{x}}(t)\|^{1/3} = \|\mathbf{f}_1(\mathbf{A}, \Phi) + \mathbf{f}_2(\mathbf{A}, \Phi, t)\|^{1/3} \tag{B3}$$

where:

$$\mathbf{f}_1(\mathbf{A}, \Phi) = \omega^3 \begin{pmatrix} \sum_n n^3 a_{y,n} a_{z,n} \sin(\varphi_{y,n} - \varphi_{z,n}) \\ \sum_n n^3 a_{x,n} a_{z,n} \sin(\varphi_{x,n} - \varphi_{z,n}) \\ \sum_n n^3 a_{x,n} a_{y,n} \sin(\varphi_{x,n} - \varphi_{y,n}) \end{pmatrix}, \quad \mathbf{A} = \begin{bmatrix} a_{x,1} & a_{y,1} & a_{z,1} \\ \cdots & & \\ a_{x,n} & a_{y,n} & a_{z,n} \end{bmatrix}, \quad \Phi = \begin{bmatrix} \varphi_{x,1} & \varphi_{y,1} & \varphi_{z,1} \\ \cdots & & \\ \varphi_{x,n} & \varphi_{y,n} & \varphi_{z,n} \end{bmatrix}$$

$$\mathbf{f}_2(\mathbf{A}, \Phi, t) = 0.5\omega^3 \begin{pmatrix} \sum_r \sum_{n \neq r} rn^2 \begin{pmatrix} a_{z,r} a_{y,n} \sin((n-r)\omega t + \varphi_{y,n} - \varphi_{z,r}) - a_{y,r} a_{z,n} \sin((n-r)\omega t - \varphi_{y,r} + \varphi_{z,n}) + \\ a_{z,r} a_{y,n} \sin((n+r)\omega t + \varphi_{y,n} + \varphi_{z,r}) - a_{y,r} a_{z,n} \sin((n+r)\omega t + \varphi_{y,r} + \varphi_{z,n}) \end{pmatrix} \\ \sum_r \sum_{n \neq r} rn^2 \begin{pmatrix} a_{x,r} a_{z,n} \sin((n-r)\omega t + \varphi_{z,n} - \varphi_{x,r}) - a_{z,r} a_{x,n} \sin((n-r)\omega t - \varphi_{z,r} + \varphi_{x,n}) + \\ a_{x,r} a_{z,n} \sin((n+r)\omega t + \varphi_{z,n} + \varphi_{x,r}) - a_{z,r} a_{x,n} \sin((n+r)\omega t + \varphi_{z,r} + \varphi_{x,n}) \end{pmatrix} \\ \sum_r \sum_{n \neq r} rn^2 \begin{pmatrix} a_{y,r} a_{x,n} \sin((n-r)\omega t + \varphi_{x,n} - \varphi_{y,r}) - a_{x,r} a_{y,n} \sin((n-r)\omega t - \varphi_{x,r} + \varphi_{y,n}) + \\ a_{y,r} a_{x,n} \sin((n+r)\omega t + \varphi_{x,n} + \varphi_{y,r}) - a_{x,r} a_{y,n} \sin((n+r)\omega t + \varphi_{x,r} + \varphi_{y,n}) \end{pmatrix} \end{pmatrix}$$

For notational convenience, all Fourier coefficients above are summarized in the matrices **A** and **F**. Ignoring the complexity of the equations for the moment, it is interesting to note that Eq. B3 can be decomposed into a time-independent term f_1 and a time varying part f_2. Importantly, this decomposition allows us to distinguish two possible strategies if the power law were used as a movement-generating principle. To obtain a time-independent, i.e., constant, *k*, a first strategy can exploit the fact that f_2 vanishes if $\mathbf{x}(t)$ is purely harmonic, i.e., for *n*=1. From our definition of smoothness, this solution is optimally smooth. Such a harmonic solution, however, has an additional property. While it is evident that two sinusoids of the same frequency and with a nonzero phase offset generate a 2D ellipse when arranged in orthogonal dimensions, also three-dimensional orthogonal oscillations of the same frequency can only produce *planar* ellipsoids in the higher dimensional space. In comparison, the results of the human and robot data show that the performed larger patterns had a 3D extension – as apparent in the increasing planarity measure with larger perimeter (see Fig. 2a). This precludes that our subjects used the harmonic solution.

As soon as $\mathbf{x}(t)$ has higher frequency components, i.e., is less smooth according to our smoothness definition, f_2 will add time-dependent variations to the slope of the *v*-*r* plot. Since f_2 has Fourier terms up to the order 2*n*–1, the Euclidean norm in Eq. B3 can increase the frequency content in *k* up to the order 2×(2*n*–1). Thus, the time course of *k* can become very complex, as it depends in subtle ways on the phases **F** and amplitudes **A**. For the case of higher-frequency components, there is theoretically a second solution for how Eq. B3 can still produce a constant *k* without the necessity of optimal smoothness. It is possible for f_2 to vanish if the higher-order Fourier terms in f_2 cancel each other. However, this solution requires precise adjustment of many parameters and is evidently a special case. It is highly improbable that this special solution is found by chance. Since our data show that the higher Fourier terms add strong time variation in the *v*-*r* plot, the special solution to achieve the power law is apparently not employed by our subjects.

In sum, if the power law were a direct criterion that the CNS uses for movement generation in Cartesian space, then trajectory generation must follow either one of the two strategies above. The "pure harmonic" solution is optimally smooth but can only produce planar patterns, while the "special solution" can lead to 3D patterns without necessarily being smooth. As it remains a fact that a lot of data in the literature, including our results on small patterns, satisfy the power law, how can these observations be reconciled with our data and analyses?

Smooth trajectories in intrinsic space can violate the power law

We pursue the hypothesis that the harmonic solution is relevant despite the fact that larger pattern produce a reduced quality of

power law fits. To develop this argument, we will focus on the robot data, since they allow direct insight into why the power law can be violated even if trajectory generation is smooth. As the robot generates movement from nothing but continuous sinusoidal oscillations in a 7-DOF joint space, trajectories are optimally smooth in *intrinsic space*. The joint space trajectories are transformed by the forward kinematics of the robot arm into an endpoint trajectory in Cartesian coordinates. For small pattern sizes, the forward kinematics f_{kin} is approximately linear:

$$\mathbf{x}(t) = \mathbf{f}_{kin}(\theta(t)) \approx J(\theta_0)\theta(t) = \begin{pmatrix} A_x \sin(\omega t + \varphi_x) + x_0 \\ A_y \sin(\omega t + \varphi_y) + y_0 \\ A_z \sin(\omega t + \varphi_z) + z_0 \end{pmatrix},$$

$$\text{where } \theta(t) = \begin{pmatrix} A_{SFE} \sin(\omega t + \varphi_{SFE}) + \theta_{0,SFE} \\ A_{SAA} \sin(\omega t + \varphi_{SAA}) + \theta_{0,SAA} \\ \cdots \\ A_{WAA} \sin(\omega t + \varphi_{WAA}) + \theta_{0,WAA} \end{pmatrix}$$

where $J(\theta_0)$ is the Jacobian of the forward kinematics. The capitalized subscripts refer to the individual joint angles and the subscript "0" denotes the constant offsets in each of the oscillations. Thus, for small patterns, the endpoint trajectory becomes a linear combination of sinusoids with different phases and amplitudes, but identical frequency ω. According to the laws of trigonometry, this linear combination results in an endpoint trajectory that remains purely harmonic and thus optimally smooth. Following the argument above, the power law must be fulfilled.

However, if the amplitudes of the joint oscillations are increased to realize large elliptical patterns, the nonlinearities of the forward kinematics come into play. Forward kinematic transformations consist of a series of multiplication of rotation matrices, each of which changes its coefficients according to the current joint angles. Thus, the sinusoidal joint trajectories are multiplied with other sinusoidal elements. Such highly nonlinear combinations of sinusoids result in an endpoint trajectory that has higher frequency components and becomes less smooth. According to Eq. B3, higher frequency components will effect that the velocity gain factor of the power is no longer constant, and the power law fit should deteriorate, as observed in our robot data. Given the striking similarity of the human and the robot data, we believe that this reasoning equally holds for the deterioration of the power law fits in our human data.

References

An CH, Atkeson CG, Hollerbach JM (1988) Model-based control of a robot manipulator. MIT Press, Cambridge, MA

Buchanan JJ, Kelso JAS, Guzman GC (1997) Self-organization of trajectory formation. I. Experimental evidence. Biol Cybern 76:257–274

Elzinga CH (1985) A note on estimation in the power law. Percept Psychophys 37:175

Flash T, Hogan N (1985) The coordination of arm movements: an experimentally confirmed mathematical model. J Neurosci 5:1688–1703

Gribble PL, Ostry DJ (1996) Origins of the power law relation between movement velocity and curvature: modeling the effects of muscle mechanics and limb dynamics. J Neurophysiol 76:2853–2860

Guzman GCd, Kelso JAS, Buchanan JJ (1997) Self-organization of trajectory formation. II. Theoretical model. Biol Cybern 76:275–284

Haggard P, Richardson J (1996) Spatial patterns in the control of human arm movements. J Exp Psychol Hum Percept Perform 22:42–62

Harris CM, Wolpert DM (1998) Signal-dependent noise determines motor planning. Nature 394:780–4

Huber PJ (1981) Robust statistics. Wiley, New York

Lacquaniti, F, Terzuolo C, Viviani P (1983) The law relating the kinematic and figural aspects of drawing movements. Acta Psychol 54:115–130

Massey JT, Lurito JT, Pellizzer G, Georgopoulos AP (1992) Three-dimensional drawings in isometric conditions: relation between geometry and kinematics. Exp Brain Res 88:685–690

Morasso P (1983) Three dimensional arm trajectories. Biol Cybern 48:187–194

Myers RH (1990) Classical and modern regression with applications. Pws-Kent, Boston, MA

Newell KM, Carlton LG (1988) Force variability in isometric responses. J Exp Psychol Hum Percept Perform 14:37–44

Osu R (1993) Coordinates for trajectory formation of human multi-joint arm movements. (IEEE Int Workshop Robot Hum Commun) IEEE, New York, pp 102–107

Press WP, Flannery BP, Teukolsky SA, Vetterling WT (1989) Numerical recipes in C: the art of scientific computing. Press Syndicate University of Cambridge, Cambridge, MA

Schaal S, Atkeson CG (1998) Constructive incremental learning from only local information. Neural Comput 10:2047–2084

Schwartz A (1994) Direct cortical representation of drawing. Science 265:540–542

Soechting JF, Terzuolo CA (1986) An algorithm for the generation of curvilinear wrist motion in an arbitrary plane in three-dimensional space. Neuroscience 19:1393–1405

Soechting JF, Lacquaniti F, Terzuolo CA (1986) Coordination of arm movements in three-dimensional space. Sensorimotor mapping during drawing movement. Neuroscience 17:295–311

Sternad D, Schaal D (1999) Segmentation of endpoint trajectories does not imply segmented control. Exp Brain Res 124:118–136

Todorov E, Jordan MI (1998) Smoothness maximization along a predefined path accurately predicts the speed profiles of complex arm movements. J Neurophysiol 80:696–714

Uno Y, Kawato M, Suzuki R (1989) Formation and control of optimal trajectory in human multijoint arm movement: minimum torque-change model. Biol Cybern 61:89–101

Viviani P, Cenzato M (1985) Segmentation and coupling in complex movements. J Exp Psychol Hum Percept Perform 11:828–845

Viviani P, Flash T (1995) Minimum-jerk, two-thirds power law, and isochrony: converging approaches to movement planning. J Exp Psychol Hum Percept Perform 21:32–53

Viviani P, Mounoud P (1990) Perceptuomotor compatibility in pursuit tracking of two-dimensional movements. J Mot Behav 22:407–443

Viviani P, Schneider R (1991) A developmental study of the relationship between geometry and kinematics in drawing movents. J Exp Psychol Hum Percept Perform 17:198–218

Viviani P, Stucchi N (1989) The effect of movement velocity on form perception: geometric illusions in dynamic displays. Percept Psychophys 46:266–274

Viviani P, Stucchi N (1992) Biological movements look uniform: evidence of motor-perceptual interactions. J Exp Psychol Hum Percept Perform 18:603–623

Viviani P, Terzuolo C (1980) Space-time invariance in learned motor skills. In: Stelmach GE, Requin J (eds) Tutorials in motor behavior. North-Holland, Amsterdam, pp 525–533

Viviani P, Terzuolo C (1982) Trajectory determines movement dynamics. Neuroscience 7:431–437

Viviani P, Campadelli P, Mounoud P (1987) Visuo-manual pursuit tracking of human two-dimensional movements. J Exp Psychol Hum Percept Perform 13:62–78

Wada Y, Kawato M (1994) Trajectory formation of arm movement by a neural network with forward and inverse dynamics models. Syst Comput Jpn 24:37–50

Wann J, Nimmo-Smith I, Wing AM (1988) Relation between velocity and curvature in movement: equivalence and divergence between a power law and a minimum jerk model. J Exp Psychol Hum Percept Perform 14:622–637

Wood JE, Meek SG, Jacobsen SC (1989) Quantitation of human shoulder anatomy for prosthetic arm control. I. Surface modelling. J Biomech 22:273–292